Applied Physics A (2021) 127:86
https://doi.org/10.1007/s00339-020-04251-5

Applied Physics A
Materials Science & Processing

Influence of the Cu substitution on magnetic properties of Ni–Mn–Sn–B shape memory ribbons

G. Kirat[1] · M. A. Aksan[2]

Received: 4 August 2020 / Accepted: 24 December 2020 / Published online: 9 January 2021

Abstract
The Heusler alloy $Ni_{50-x}Cu_xMn_{38}Sn_{12}+B_y$ ($x=0$, 1, 3 and 5) was successfully produced in ribbon form using melt spinning technique. The magnetic properties of the obtained ribbons were analyzed in detail. In all ribbons, it was detected that the ferromagnetic austenite phase transformed into the weak magnetic martensite phase. A separation between FC and ZFC curves at lower temperatures was found. An increase in the magnetization in FC mode can be attributed to the coexistence of ferromagnetic (FM)/antiferromagnetic (AFM) at martensitic phase. It was found that the transition temperatures shifted to low temperatures with increasing the Cu content. The magnetization results under high magnetic field (10 kOe and 50 kOe) showed a thermal hysteresis between the cooling and heating cycles, which is clear evidence for a first-order transformation in the ribbons. From M–H data, all the ribbons exhibited ferromagnetic behavior at low temperatures below the martensitic transition temperature and paramagnetic behavior at high temperatures above the transition temperature. The results provide us a comprehensive view to reveal the effect of the Cu substitution on the magnetic properties of Ni–Mn-based shape memory ribbons.

Keywords Shape memory alloys · Ni–Mn–Sn · Magnetic properties · Ribbons

1 Introduction

The shape memory Heusler alloys are of great interest due to good magneto-functional properties such as magnetocaloric effect (MCE) [1, 2], barocaloric effect [3], elastocaloric effect [4], magnetic field-induced shape recovery magnetostrain effect [5], giant magnetoresistance effect [6, 7] and kinetic arrest [8], which rely on magnetic and structural phase transition occurred at the same temperature. An applied magnetic field leads to stabilization of the high-temperature austenite phase. Difference between Zeeman energy of austenite phase and that of martensite phase causes a large change in magnetization during the martensitic transition which is evidence of a field-induced martensitic transformation (FIMT) [9]. A large entropy change and a good magnetocaloric effect occur due to the large magnetization change. Therefore, application of the magnetic field enables the production of new generation actuators and sensors that can be used in high-frequency applications or magnetic cooling devices.

For the technological applications of these materials, the martensitic transition (T_M) temperature should be close to room temperature. Many experimental studies are carried out to tune the martensitic transition temperature. It is well known that the T_M temperature is extremely sensitive to the stoichiometry of the material. Therefore, the most commonly used method to tune the T_M temperature is to change the composition stoichiometry and to substitute/dope various elements to the host material.

Ni–Mn–X (X = In, Sn or Sb)-based alloys are the ideal materials to investigate the magnetic field-induced martensitic transition (MFIMT) properties and possible technological applications such as actuators and sensors. Ni–Mn–X-based alloys undergo a first-order phase transition from a cubic austenite phase with high symmetry to a martensite phase with lower symmetry. It has been found that the change of stoichiometry and the doping of various elements modify the T_M temperature and the magnetostructural properties of the alloys, which is essential for technological applications. The

✉ M. A. Aksan
mehmet.aksan@inonu.edu.tr

[1] Inonu Universitesi, Scientific and Technological Research Center, 44280 Malatya, Turkey

[2] Fen Edebiyat Fakultesi, Inonu Universitesi, Fizik Bolumu, 44280 Malatya, Turkey

magnetostructural properties are very sensitive to the Mn content in the Ni–Mn–X system; the excess Mn atoms in the $Ni_2Mn_{1+x}X_{1-x}$ system can occupy the different sites in unit cell, which causes structural instability [10, 11]. This instability leads to the ferromagnetic shape memory effect. It is also known that in the excess Mn-containing $Ni_2Mn_{1+x}X_{1-x}$ system, short-range antiferromagnetic (AFM) arrangement between the excess Mn at the X site and the original Mn atoms occurs [11–13].

In the Ni–Mn–Sn-based Heusler alloys, the alloy crystallizes in the $L2_1$ cubic structure [10, 14]. Magnetic ordering, magnetostructural and magneto-transport properties in the Ni-Mn-Sn Heusler alloys were found to depend on the composition and fabrication conditions. In Mn-rich alloys, the excess Mn atoms occupy the Sn sites and the antiferromagnetic arrangement between the original Mn sites and the surrounding Mn atoms occurs [10, 15]. When the stoichiometry of the Ni–Mn–Sn alloy is optimized, the large inverse magnetocaloric effect (MCE) is observed due to the different exchange interactions between martensite phase and austenite phase, which lead to a large change in the magnetization [16–18].

In order to shift the T_M temperatures and to reduce the degree of hysteresis associated with the structural martensitic transition, some elements, such as Co, Cu and Pd, have been substituted/doped to the off-stoichiometric Ni–Mn–Sn system [9, 19–21]. It was found that Cu substitution has significant effects on the properties of the Ni–Mn–Sn system; the Cu substitution for Mn and Sn caused a shift of the martensitic transition to high temperatures [7, 9, 22, 23], while the transition with the Cu substitution for Ni shifted to low temperatures [24, 25]. Since Cu is non-magnetic, the exchange interactions in the system reduce and thus Curie temperature shifts to low temperatures.

The fact that the shape memory Heusler alloys in bulk form are brittle and not flexible enough, which are originated from the highly ordered intermetallic Heusler structure, limits the technological applications of these materials. Therefore, it is necessary to produce flexible and almost single crystalline materials. Ribbons are appropriate materials that meet these requirements. A continuous and large-mass ribbon production can be easily achieved by the melt spinning technique. Long and high-temperature annealing process conditions can be eliminated or reduced by this technique. So, single-phase alloys with suitable functional properties can be obtained.

A detailed investigation of the magnetic properties of ribbons is extremely important in terms of their application to technological/industrial fields. In this paper, the effect of systematic non-magnetic Cu substitution on the magnetic field-induced martensite properties of Ni–Mn–Sn–B-based shape memory ribbons has been studied. $Ni_{50-x}Cu_xMn_{38}Sn_{12}+B_y$ ($x=0$, 1, 3 and 5) ribbons have been prepared using melt spinning technique and the magnetic properties of the ribbons analyzed in detail. It should be mentioned that boron (B) was added to the Ni–Mn–Sn alloys to prevent quick Mn evaporation because of its small atomic radius [26, 27].

2 Experimental procedure

Ingots with nominal stoichiometry of $Ni_{50-x}Cu_xMn_{38}Sn_{12}+B_y$ ($x=0$, 1, 3 and 5) were produced in a water-cooled Cu crucible using an arc melter. The production process was carried out in argon atmosphere. The ribbons (~5–6 mm width, ~20–25 mm length and ~15–20 μm thickness, respectively) were fabricated using the ingots in a melt spinner. The materials obtained were annealed at 1173 K for 2 h for homogenization and then quenched in ice water. This procedure offers several advantages such as the synthesis of nearly single-phase, highly textured samples and shortened annealing stage. The ribbons were marked as RS ($x=0.0$), RB1 ($x=1.0$), RB3 ($x=3.0$) and RB5 ($x=5.0$), respectively. It should be emphasized that Mn in the Ni–Mn–X system can quickly evaporate during heat treatments. Therefore, in this study, we added boron to the host material to prevent Mn evaporation. From our previous experiences [14, 28], optimum boron content in the system was found to be 3% at. The composition of the ribbons was estimated to be $Ni_{50}Mn_{38}Sn_{12}+B_x$, $Ni_{49}CuMn_{38}Sn_{12}+B_x$, $Ni_{47}Cu_3Mn_{38}Sn_{12}+B_x$ and $Ni_{45}Cu_5Mn_{38}Sn_{12}+B_x$ for $x=0$, 1.0, 3.0 and 5.0, respectively, using scanning electron microscope–energy-dispersive X-ray (SEM–EDX) analysis.

X-ray diffraction (XRD) analyses were performed using CuK_α radiation ($\lambda=1.5405$ Å) with scanned range of $30° \le 2\theta \le 80°$ and scan speed of 2° min^{-1}. Magnetization measurements were performed between 0 and 90 kOe using a Quantum Design PPMS-90 kOe system with the vibrating sample magnetometer (VSM) attachment. Magnetic field was applied parallel to the ribbon surface during the measurements.

3 Results and discussion

XRD patterns of the ribbons fabricated are shown in Fig. 1. It was identified that the Cu substitution did not cause a change in the structural properties. The ribbons were found to possess the cubic bcc $L2_1$ phase of the Ni–Mn–Sn system. However, near $2\theta \cong 44°$, a secondary phase was also detected as Mn_2B, but its intensity is very low compared to the cubic bcc $L2_1$ phase.

The unit cell parameter, a, for RS, RB1, RB3 and RB5 ribbons, was found to be 0.5967 nm (±0.5%), 0.5970 nm (±0.5%), 0.5973 nm (±0.5%) and 0.5976 nm (±0.5%), respectively, using Rietveld refinement. It is seen that there

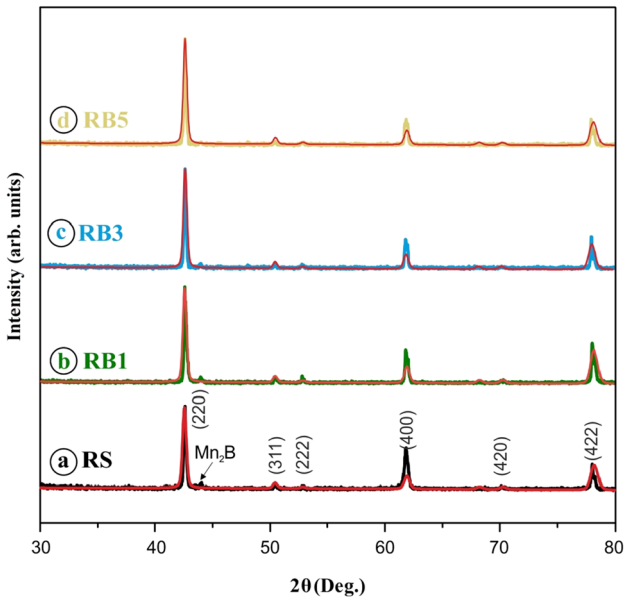

Fig. 1 XRD patterns of **a** RS, **b** RB1, **c** RB3 and **d** RB5 ribbons. Red lines show Rietveld refinement result

is an increase in the parameter *a* with increasing the Cu content, which indicates an expansion in the unit cell. If we consider that Cu^{2+} atoms occupy exactly Ni^{2+} sites, we believe that this expansion in the unit cell is caused by larger ionic radius of Cu^{2+} (0.128 nm) than that of Ni^{2+} (0.125 nm) [29].

Temperature dependence (M–T) of field-cooled (FC) and zero-field-cooled (ZFC) magnetization of the unsubstituted (RS) and Cu-substituted ribbons (RB1, RB3 and RB5) under the magnetic field of 100 Oe is shown in Fig. 2. During the ZFC experiments, the ribbons were initially cooled to

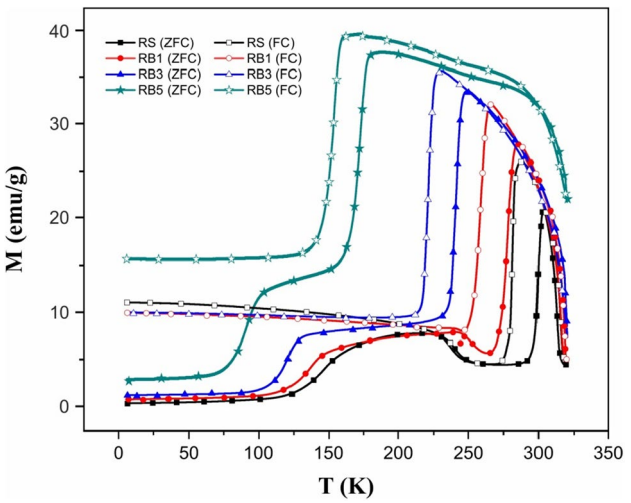

Fig. 2 Temperature dependence of field-cooled (FC) and zero-field-cooled (ZFC) magnetization of the ribbons under the magnetic field of 100 Oe

50 K at zero magnetic field and then the measurements were performed during heating runs under a magnetic field of 100 Oe. In the FC experiments, the ribbons were cooled under magnetic field of 100 Oe. The magnetic field during both experiments is directed along the ribbons surface. Phase transition temperatures obtained in FC and ZFC mode are listed in Table 1. Magnetic transition temperatures were determined by the x-axis intercept of the tangent line to the steepest slope of the peaks in the M–T curves [30]. It should be mentioned that the uncertainty of these temperatures is about 1 K.

Two important points should be pointed out here: First, the magnetization of the ribbons in FC measurements was higher than that of ZFC measurements. Second, a hysteresis occurred between FC and ZFC data. In the ZFC mode, when the temperature was decreased from high-temperature region, the magnetization increased abruptly and a peak in the magnetization was attained, which corresponds to transition from the paramagnetic austenite phase to the ferromagnetic austenite phase [31]. The abrupt decrease in the magnetization with further decreasing the temperature suggests the austenite–martensite phase transition. A similar magnetization behavior was observed in the FC curve. It should be emphasized that the austenite–martensite transition accompanied by a thermal hysteresis between FC and ZFC curves indicates the first-order phase transition. It was reported [6, 20, 32] that the abrupt decrease in the magnetization may be caused by the onset of the antiferromagnetic ordering around the ferromagnetic austenite peak. Antiferromagnetism arises from the nearest neighbor Mn–Mn pairs in the martensite phase [20, 33, 34]. In the Ni–Mn-based Heusler alloys, the magnetization is mainly caused by Mn atoms. The Ruderman–Kittel–Kasuya–Yosida (RKKY) exchange that occurs through the conducting electrons leads to a ferromagnetic ordering. But, in the Heusler alloys having excess Mn content, the distance between nearest Mn atoms is shortened and antiferromagnetic Mn–Mn arrangement occurs. The competition between ferromagnetic and antiferromagnetic ordering leads to the weak ferromagnetism of the martensitic state [35].

It was seen that the magnetization rises slightly around 250 K in ZFC curves, which can be attributed to be paramagnetic transition in the martensite phase [36, 37]. It

Table 1 Phase transition temperatures in ZFC and FC mode

Ribbon	ZFC		FC	
	A_s (K)	A_f (K)	A_s (K)	A_f (K)
RS	302	289	291	284
RB1	285	266	273	254
RB3	243	221	238	262
RB5	177	155	167	146

should be pointed out that any magnetization rise in RB3 and RB5 ribbons was not obtained. Around 150 K, a prominent decrease in the magnetization was observed which is believed to correspond to the antiferromagnetic state. Xuan et al. reported that the excess Mn atoms in the $Mn_{50}Ni_{38}Sn_{12}$ system will most likely occupy the Ni and Sn sites and the magnetic moments of the Mn atoms on the Ni and Sn sites are coupled antiferromagnetically to those of Mn atoms on the Mn sites [10, 15]. But antiferromagnetic contribution compared to the other magnetic ones is very small.

A visible separation between FC and ZFC curves at low temperatures (below 250 K) was observed. The magnetization in FC mode tends to increase with lowering of temperature, which indicates the coexistence of ferromagnetic (FM)/antiferromagnetic (AFM) at martensitic phase [38]. As mentioned above, the antiferromagnetic ordering arises from the antiferromagnetic coupling between Mn atoms in the Mn sites and the Mn atoms that occupy the Ni and Sn sites. In ZFC mode, the ferromagnetic spin structures are pinned by antiferromagnetic zones, which lead to low magnetization state below 150 K. In FC mode, the Zeeman energy which supplies by external field can overcome the exchange coupling of the FM/AFM and then a separation between ZFC and FC curves occurs at lower temperatures.

It was found that there is a compositional dependence on transition temperatures. The transition temperatures significantly shifted to the low temperatures with increasing the Cu content in the Ni–Mn–Sn + B system, as shown in Table 1.

Figure 3a and b shows the M–T curves of the ribbons at 10 kOe (1 T) and 50 kOe (5 T). Contrary to the measurements at 100 Oe magnetic field, the ribbons showed distinct ferromagnetic behavior in high magnetic field measurements. Under both 50 kOe and 10 kOe magnetic fields, it was observed that a phase transformation from ferromagnetic austenite to weak ferromagnetic martensite in the cooling stage occurs, which is attributed to magnetostructural transformation (Fig. 3a and b). During martensitic transition, a rapid decrease in magnetization was found due to the lower saturation magnetization of martensite than ferromagnetic austenite [16, 39].

A sudden increase in M–T curves on the heating stage was observed, which is associated with the reverse transformation. A thermal hysteresis was obtained between the cooling and heating M–T data. It is worth mentioning that the martensitic transformation in the ribbons is a first-order transformation which is represented by thermal hysteresis that is typical for martensitic–austenite transformation.

Transformation temperatures at high magnetic fields are listed in Table 2. Two important results can be derived from Table 2: (1) Transformation temperatures decreased by the Cu substitution. (2) The transformation temperatures also decreased with the applied magnetic field. Shift of the magnetic field-induced structural transition temperatures is a characteristic feature of metamagnetic Ni–Mn–X (X = In, Sn and Sb) shape memory alloys. In the case of high level of the Cu substitution and high magnetic fields applied (10 kOe and 50 kOe), the martensitic transformation is completed at the very low temperatures, for example near 150 K in the RB5 sample. Studies on the decrease in MT temperature with substitution/doping to Ni–Mn-based alloys and ribbons can be found in the literature [7, 40–42].

The temperature range for the martensitic transformation, $\Delta T_{A\text{-}M}$, can be derived using

$$\Delta T_{A-M} = \frac{(A_f - A_s) + (M_s - M_f)}{2}$$

where A_s, A_f, M_s and M_f are the starting and finishing temperatures of the austenite and martensitic phase, respectively

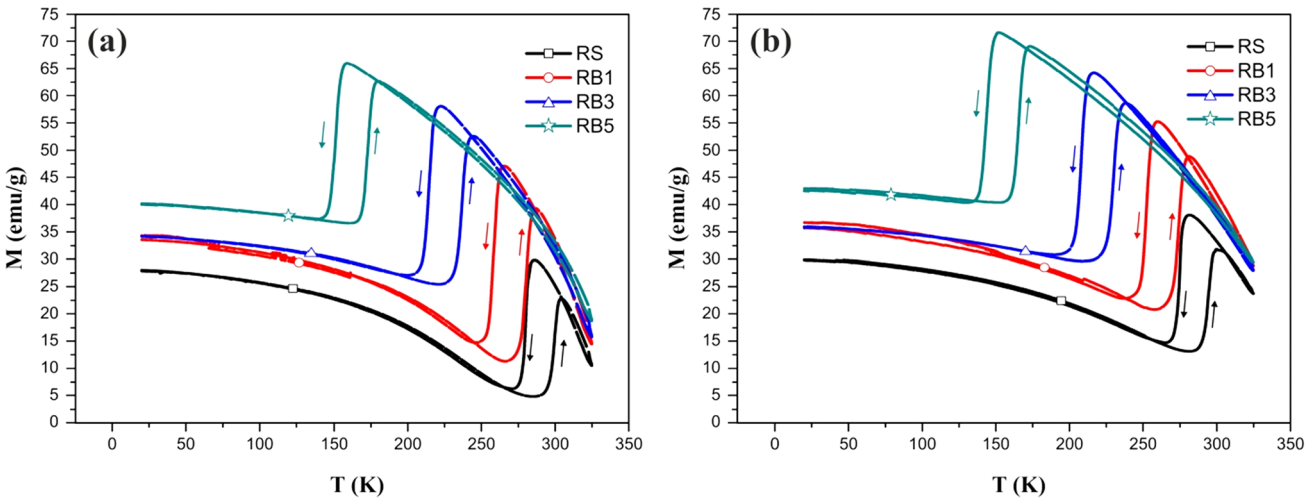

Fig. 3 Temperature dependence of magnetization of RS, RB1, RB3 and RB5 ribbons at (**a**) 10 kOe and (**b**) 50 kOe

Table 2 Phase transformation temperatures of RS, RB1, RB3 and RB5 ribbons at the magnetic field of 10 kOe and 50 kOe

Ribbon	A_s (K)	A_f (K)	ΔA (= $A_f - A_s$) (K)	M_s (K)	M_f (K)	ΔM (= $M_s - M_f$) (K)	$\Delta T_{A\text{-}M}$ (K)
For 10 kOe							
RS	290	304	14	286	272	14	14.0
RB1	267	286	19	265	246	19	19.0
RB3	227	244	17	222	207	15	16.0
RB5	165	173	8	158	143	15	11.5
For 50 kOe							
RS	285	301	16	282	265	17	16.5
RB1	259	281	22	260	240	20	21.0
RB3	218	239	21	216	198	18	19.5
RB5	157	173	15	151	136	15	15.5

[43]. The calculated $\Delta T_{A\text{-}M}$ values are given in Table 2. The widest $\Delta T_{A\text{-}M}$ and so the corresponding thermal hysteresis were obtained in RB1 ribbon and decreased with increasing the Cu content in the Ni–Mn–Sn–B system. A plausible explanation on the decrease in $\Delta T_{A\text{-}M}$ is the increase in atomic order degree (AOD) with the Cu substitution [43].

Shift of the martensitic transformation temperatures to low temperatures with the element substitution/doping to the Ni–Mn–Sn-based shape memory alloys arises from the variation of the valence electron concentration per atom, *e/a*, or the formation of the second phase, or the change of Mn–Mn distance [44, 45]. *e/a* was calculated to be 7.99, 8.00, 8.01 and 8.03 for RS, RS1, RS3 and RS5 ribbons, respectively. It is obvious that the substitution of Cu for Ni causes a slight increase in the value *e/a*, which should lead to an increment in the phase transformation temperatures. On contrary, the phase transformation temperatures decreased by the Cu–substitution in the present study. Therefore, the shift of phase transformation temperatures cannot be explained in terms of the value *e/a*. In conjunction with XRD results, we believe that the substitution of Cu^{2+} (0.128 nm) with larger ionic radius compared to Ni^{2+} (0.125 nm) increases the unit cell volume. This results in the increase in the Mn–Mn distance (d_{Mn-Mn}), which leads to shift of phase transformation temperatures to low temperatures [46]. Furthermore, the increase in Mn–Mn bond lengths also causes a decrease in hybridization between Ni-3d and Mn-d states, which can also lead to a decrease in MT temperature [47].

Magnetization versus applied magnetic field (M–H) curves of the ribbons at different temperatures are presented in Fig. 4a–d. It was found that all the ribbons exhibited ferromagnetic behavior with saturation fields less than 10 kOe at 10 K and 100 K. Any saturation was not reached at the measurements at 325 K which is in the austenite phase region. When considering together with the M–T results obtained under the magnetic field of 100 Oe, a linear dependence on the applied magnetic field at 325 K clearly indicates predominant paramagnetic behavior in the austenite region. It is worth noting that above certain magnetic field, the linear increment of the magnetization with the applied magnetic field suggests a predominant paramagnetic behavior. But below it, the shape of the hysteresis loops indicates the existence of ferromagnetic interactions. It was identified that the Cu-substituted ribbons (RB1, RB3 and RB5) keep similar magnetic behavior to the unsubstituted ribbon (RS). Notice that the Cu substitution caused slight increment of the magnetization of saturation.

For the sake of clarity, M–H results of the ribbons at temperatures in the phase transition region in Fig. 2 are shown in Fig. 5. In each measurement, the sample was first cooled to the martensite phase (below the M_f temperature) and then reheated. The M–H data were taken by field-up from 0 to 90 kOe and then by field-down from 90 to 0 kOe. Magnetic hysteresis observed between field-up and field-down process confirms metamagnetic-like behavior near the austenite–martensite transformation in the ribbons. The shape of M–H curves changed with increasing the Cu content in the Ni–Mn–Sn–B system. It was seen that the magnetic hysteresis gets narrow by the Cu substitution, especially in the RB5 ribbon. An increase in the magnetization value and the narrow thermal hysteresis in the RB5 ribbon indicate that the magnetostructural transformation occurs in low magnetic fields.

4 Conclusion

In conclusion, we have evaluated the magnetic properties of the ribbons with stoichiometry of $Ni_{50-x}Cu_xMn_{38}Sn_{12} + B_y$ ($x = 0$, 1.0, 3.0 and 5.0). Fabrication of the Ni–Mn–Sn alloys in the ribbon form using melt spinning technique provides an advantage in terms of obtaining materials with optimum magnetic properties

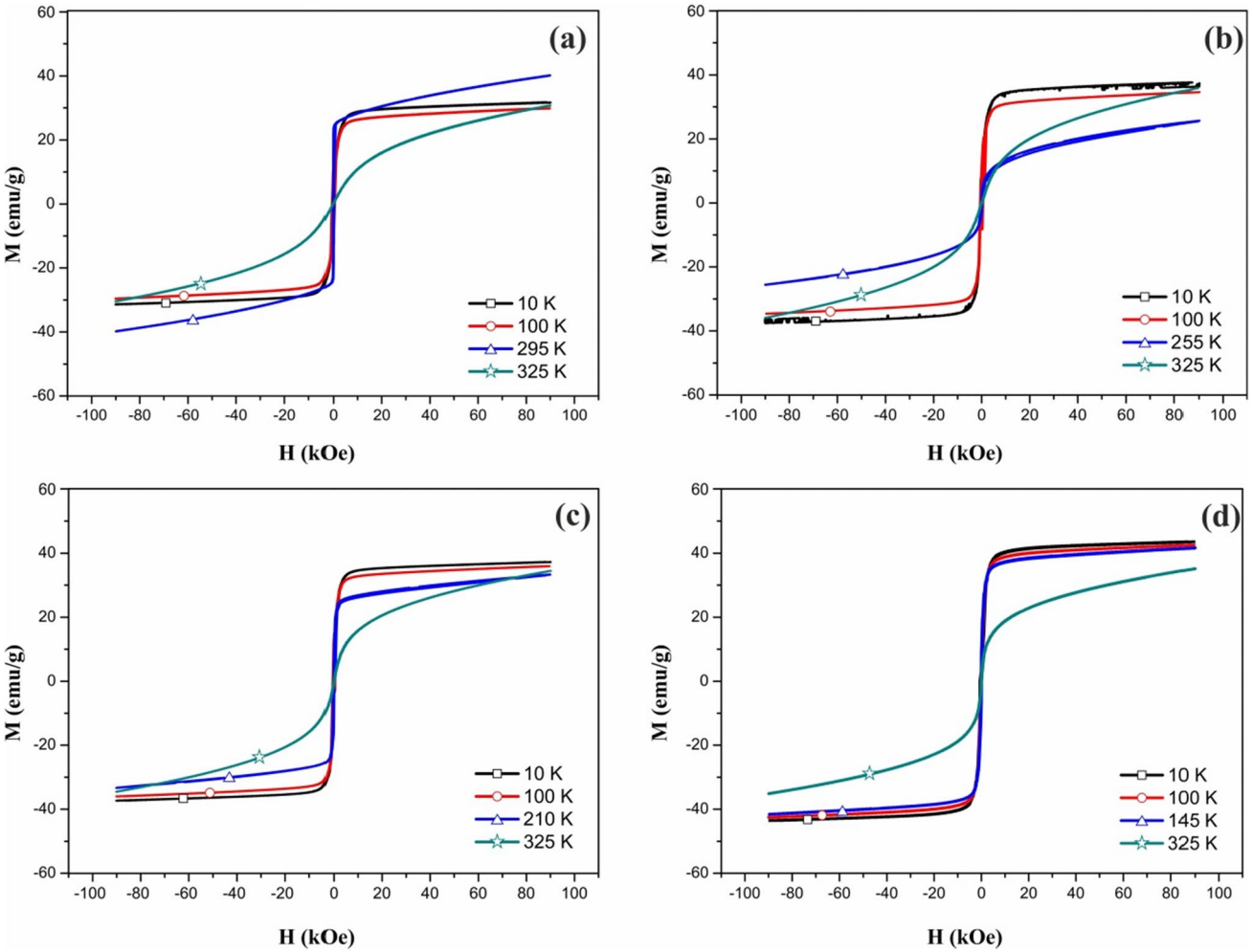

Fig. 4 M–H results of **a** RS, **b** RB1, **c** RB3 and **d** RB5 ribbons at different temperatures

for its potential use in technological applications such as actuators, sensors or magnetic refrigerants. In this study, it was found that the magnetic field has profound influence on the martensitic transition. The results clearly suggest that the magnetic field-induced first-order transition exists in the ribbons fabricated. With the Cu substitution, the martensitic transition temperature shifted to low temperatures, which is believed to be due to increase in the Mn–Mn distance (d_{Mn-Mn}). Ribbons exhibited sharp austenite–martensite phase transition. The magnetization of ribbons increased with increasing the Cu content. The M–H results reveal that paramagnetic behavior in the ribbons with the magnetic field applied over a certain magnetic field occurs, but ferromagnetic interactions below it.

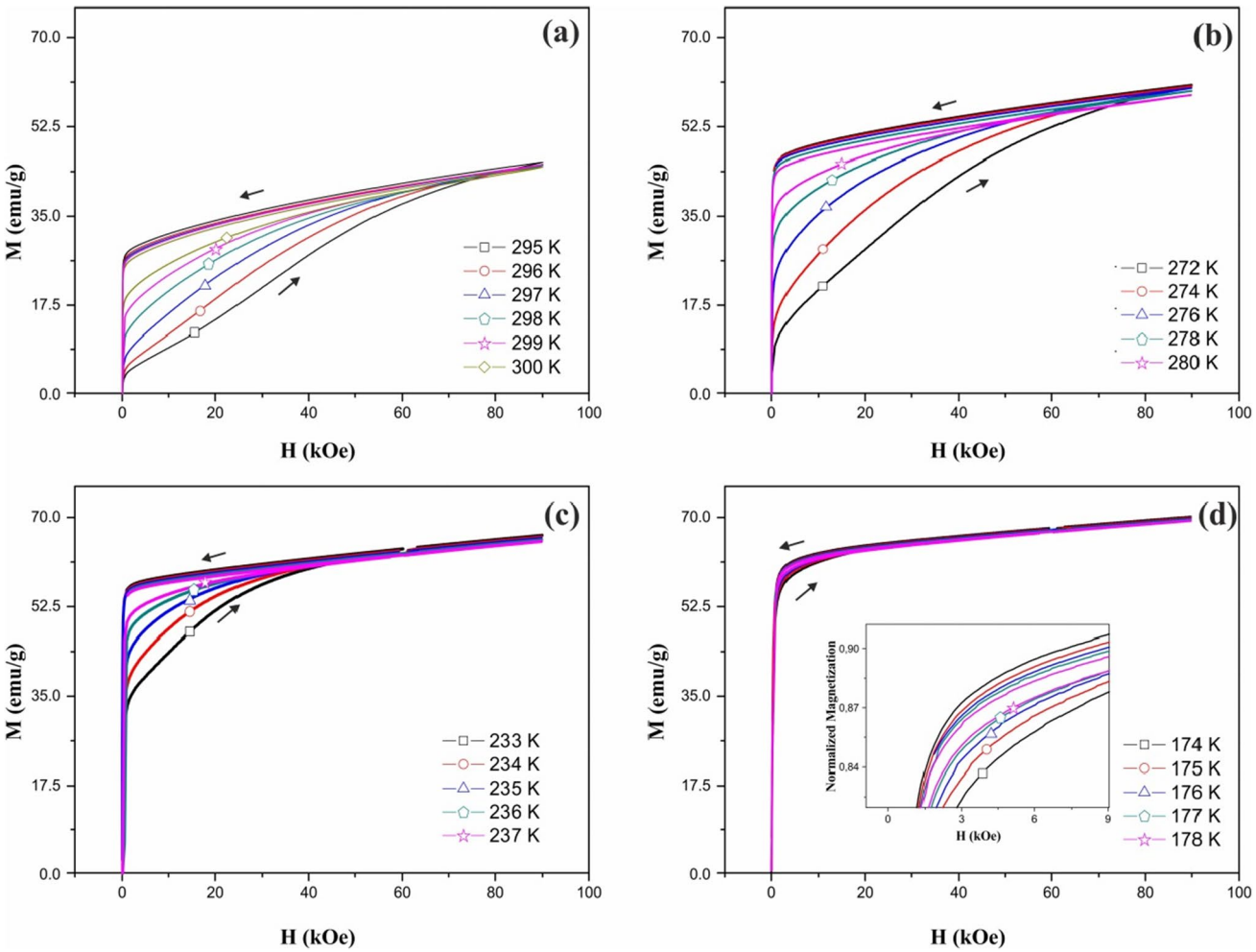

Fig. 5 M–H curves of **a** RS, **b** RB1, **c** RB3 and **d** RB5 at temperatures in the phase transition region

Acknowledgment This work was supported by the Research Fund of Inonu University, Turkey, under Grant Contract No. FBA-2020-2016.

References

1. F. Chen, J.L. Sánchez Llamazares, C.F. Sánchez-Valdés, P. Müllner, Y.X. Tong, L. Li, Wide structural and magnetic successive transitions and related magnetocaloric properties in a directionally solidified polycrystalline Ni–Co–Mn–In alloy. Shap. Mem. Superelasticity, **6**, 54–60 (2020).
2. S. Stadler, M. Khan, J. Mitchell, N. Ali, A.M. Gomes, I. Dubenko, A.Y. Takeuchi, A.P. Guimarães, Magnetocaloric properties of $Ni_2Mn_{1-x}Cu_xGa$. Appl. Phys. Lett. **88**, 192511 (2006)
3. L. Manosa, D. Gonzalez-Alonso, A. Planes, E. Bonnot, M. Barrio, J.L. Tamarit, S. Aksoy, M. Acet, Giant solid-state barocaloric effect in the Ni-Mn-In magnetic shape-memory alloy. Nature Mater. **9**, 478–481 (2010)
4. B. Lu, F. Xiao, A. Yan, J. Liu, Elastocaloric effect in a textured polycrystalline Ni-Mn-In-Co metamagnetic shape memory alloy. Appl. Phys. Lett. **105**(16), 161905 (2014)
5. R. Kainuma, Y. Imano, W. Ito, Y. Sutou, H. Morito, S. Okamoto, O. Kitakami, K. Oikawa, A. Fujita, T. Kanomata, K. Ishida, Magnetic-field-induced shape recovery by reverse phase transformation. Nature (London) **439**, 957–960 (2006)
6. B. Borgohain, P.K. Siwach, N. Singh, K.V.R. Rao, H.K. Singh, Magnetic and magnetotransport characteristics of Cr-substituted $Ni_{55}Mn_{34}Sn_{11}$ thin films grown by magnetron sputtering. J. Supercond. Nov. Magn. **32**, 3295–3304 (2019)
7. C. Jing, Y.J. Yang, Z. Li, X.L. Wang, B.J. Kang, S.X. Cao, J.C. Zhang, J. Zhu, B. Lu, Tuning martensitic transformation and large

magnetoresistance in $Ni_{50-x}Cu_xMn_{38}Sn_{12}$ Heusler alloys. J. Appl. Phys. **113**, 173902 (2013)
8. N.M. Bruno, D. Salas, S. Wang, Igor V. Roshchin, R. Santamarta, R. Arroyave, T. Duong, Y.I. Chumlyakov, I. Karaman, On the microstructural origins of martensitic transformation arrest in a NiCoMnIn magnetic shape memory alloy. Acta Mater., **142**, 95–106 (2018)
9. Wederni A, M. Ipatov, E. Pineda, J.-J. Suñol, L. Escoda, J.M. González, S. Alleg, M. Khitouni, R. Żuberek, O. Chumak, A. Nabiałek, A. Lynnyk, Magnetic properties, martensitic and magnetostructural transformations of ferromagnetic Ni-Mn-Sn-Cu shape memory alloys. Appl. Phys. A, **126**, 320 (2020).
10. H.C. Xuan, Q.Q. Cao, C.L. Zhang, S.C. Ma, S.Y. Chen, D.H. Wang, Y.W. Du, Large exchange bias field in the Ni-Mn-Sn Heusler alloys with high content of Mn. Appl. Phys. Lett. **96**, 202502 (2010)
11. T. Krenke, M. Acet, E.F. Wassermann, X. Moya, L. Mañosa, A. Planes, Martensitic transitions and the nature of ferromagnetism in the austenitic and martensitic states of Ni-Mn-Sn alloys. Phys. Rev. B **72**, 014412 (2005)
12. S. Chatterjee, S. Giri, S.K. De, S. Majumdar, Reentrant spin glass state in Mn doped Ni_2 MnSn shape memory alloy. https://arxiv.org/abs/0812.1115. (2008)
13. J. Enkovaara, O. Heczko, A. Ayuela, R.M. Nieminen, Coexistence of ferromagnetic and antiferromagnetic order in Mn-doped Ni_2MnGa. Phys. Rev. B **67**, 212405 (2003)
14. G. Kirat, M.A. Aksan, Y. Aydogdu, Magnetic field induced martensitic transition in Fe doped Ni-Mn-Sn-B shape memory ribbons. Intermetallics **111**, 106493 (2019)
15. N. Singh, B. Borgohain, A.K. Srivastava, A. Dhar, H.K. Singh, Magnetic nature of the austenite–martensite phase transition and spin glass behaviour in nanostructured $Mn_2Ni_{1.6}Sn_{0.4}$ melt-spun ribbons. Appl. Phys. A **122**, 237 (2016).
16. B. Hernando, J.L. Sánchez Llamazares, J.D. Santos, V.M. Prida, D. Baldomir, D. Serantes, R. Varga, J. González, Magnetocaloric effect in melt spun $Ni_{50.3}Mn_{35.5}Sn_{14.4}$ ribbons. Appl. Phys. Lett., **92**, 132507 (2008).
17. Z.D. Han, D.H. Wang, C.L. Zhang, H.C. Xuan, B.X. Gu, Y.W. Du, Low-field inverse magnetocaloric effect in $Ni_{50-x}Mn_{39+x}Sn_{11}$ Heusler alloys. Appl. Phys. Lett. **90**, 042507 (2007)
18. P.A. Bhobe, K.R. Priolkar, A.K. Nigam, Room temperature magnetocaloric effect in Ni-Mn-In. Appl. Phys. Lett. **91**, 242503 (2007)
19. X. Zhang, H. Zhang, M. Qian, L. Geng, Enhanced magnetocaloric effect in Ni-Mn-Sn-Co alloys with two successive magnetostructural transformations. Sci. Rep. **8**, 8235 (2018)
20. P.O. Castillo-Villa, L. Mañosa, A. Planes, D.E. Soto-Parra, J.L. Sánchez-Llamazares, H. Flores-Zúñiga, C. Frontera, Elastocaloric and magnetocaloric effects in Ni-Mn-Sn(Cu) shape-memory alloy. J. Appl. Phys. **113**, 053506 (2013)
21. R. Saha, A.K. Nigam, Room temperature inverse magnetocaloric effect in Pd substituted $Ni_{50}Mn_{37}Sn_{13}$ Heusler alloys. Phys. B **448**, 263 (2014)
22. D.H. Wang, C.L. Zhang, H.C. Xuan, Z.D. Han, J.R. Zhang, S.L. Tang, B.X. Gu, Y.W. Du, The study of low-field positive and negative magnetic entropy changes in $Ni_{43}Mn_{46-x}Cu_xSn_{11}$ alloys. J. Appl. Phys. **102**, 013909 (2007)
23. R. Das, S. Sarma, A. Perumal, A. Srinivasan, Effect of Co and Cu substitution on the magnetic entropy change in $Ni_{46}Mn_{43}Sn_{11}$ alloy. J. Appl. Phys. **109**, 07A901 (2011)
24. K. Zhang, X. Tian, C. Tan, E. Guo, W. Zhao, W. Cai, K. Zhang, X. Tian, C. Tan, E. Guo, W. Zhao, W. Cai, Designing a new Ni-Mn-Sn ferromagnetic shape memory alloy with excellent performance by Cu addition. Metals **8**, 152 (2018)
25. Dincer I, E. Yuzuak, Y. Elerman, Influence of irreversibility on inverse magnetocaloric and magnetoresistance properties of the $(Ni,Cu)_{50}Mn_{36}Sn_{14}$ alloys. J. Alloys Compd. **506**, 508–512 (2010).
26. S. Kavita, V.V. Ramakrishna, P. Yadav, S. Kethavath, N.P. Lalla, T. Thomas, P. Bhatt, R. Gopalan, Enhancement of martensite transition temperature and inverse magnetocaloric effect in $Ni_{43}Mn_{47}Sn_{11}$ alloy with B doping. J. Alloys Compd. **795**, 519–527 (2019)
27. Y. Aydogdu, A.S. Turabi, A. Aydogdu, M. Kok, Z.D. Yakinci, H.E. Karaca, The effects of boron addition on the magnetic and mechanical properties of NiMnSn shape memory alloys. J. Therm. Anal. Calorim. **126**, 399–406 (2016)
28. G. Kirat, O. Kizilaslan, M.A. Aksan, Magnetoresistance properties of magnetic Ni-Mn-Sn-B shape memory ribbons and magnetic field sensor aspects operating at room temperature. J. Magn. Magn. Mater. **477**, 366–371 (2019)
29. Wojcik A, W. Maziarz, M.J. Szczerba, M. Sikora, A. Zywczak, C.O. Aguilar-Ortiz, P. Alvarez-Alonso, E. Villa, H. Flores-Zúniga, E. Cesari, J. Dutkiewicz, V.A. Chernenko, Transformation behavior and inverse caloric effects in magnetic shape memory $Ni_{44-x}Cu_xCo_6Mn_{39}Sn_{11}$ ribbons. J. Alloys Compd. **721**, 172–181 (2017)
30. W.M. Yuhasz, D.L. Schlagel, Q. Xing, R.W. McCallum, T.A. Lograsso, Metastability of ferromagnetic Ni–Mn–Sn Heusler alloys. J. Alloys Compd. **492**, 681–684 (2010)
31. K. Fukushima, K. Sano, T. Kanomata, H. Nishihara, Y. Furutani, T. Shishido, W. Ito, R.Y. Umetsu, R. Kainuma, K. Oikawa, K. Ishida, Phase diagram of Fe-substituted Ni-Mn-Sn shape memory alloys. Scripta Mater. **61**, 813–816 (2009)
32. S. Aksoy, M. Acet, P.P. Deen, L. Manosa, A. Planes, Magnetic correlations in martensitic Ni-Mn-based Heusler shape-memory alloys: Neutron polarization analysis. Phys. Rev. B **79**, 212401 (2009)
33. V.D. Buchelnikov, P. Entel, S.V. Taskaev, V.V. Sokolovskiy, A. Hucht, M. Ogura, H. Akai, M.E. Gruner, S.K. Nakay, Monte Carlo study of the influence of antiferromagnetic exchange interactions on the phase transitions of ferromagnetic Ni-Mn-X alloys (X=In, Sn, Sb). Phys. Rev. B **78**, 184427 (2008)
34. V.V. Sokolovskiy, V.D. Buchelnikov, M.A. Zagrebin, P. Entel, S. Sahool, M. Ogura, First-principles investigation of chemical and structural disorder in magnetic $Ni_2Mn_{1+x}Sn_{1-x}$ Heusler alloys. Phys. Rev. B **86**, 134418 (2012)
35. B. Gao, J. Shen, F.X. Hu, J. Wang, J.R. Sun, B.G. Shen, Magnetic properties and magnetic entropy change in Heusler alloys $Ni_{50}Mn_{35-x}Cu_xSn_{15}$. Appl. Phys. A **97**, 443–447 (2009)
36. Z. Wu, J. Guo, Z. Liang, Y. Zhang, X. Ye, J. Zhang, Y. Li, Y. Liu, H. Yang, Room temperature metamagnetic transformation of a tough dual-phase Ni-Mn-Sn-Fe ferromagnetic shape memory alloy. J. Alloys Compd. **829**, 154606 (2020)
37. J.J. Suñol, J. Saurina, R. Varga, B. Hernando, J.L. Sánchez-Llamazares, J.D. Santos, V.M. Prida, Structural and magnetic transitions in rapidly solidified Heusler alloys ribbons. Solid State Phenom. **150**, 143–157 (2009)
38. C. Jing, Z. Li, H.L. Zhang, J.P. Chen, Y.F. Qiao, S.X. Cao, J.C. Zhang, Martensitic transition and inverse magnetocaloric effect in Co doping Ni–Mn–Sn Heusler alloy. Eur. Phys. J. B **67**, 193–196 (2009)
39. Y. Shen, W. Sun, Z. Wei, J. Li, J. Guo, K. Wang, Y. Zhang, J. Liu, Influence of microstructure on elastocaloric and shape memory effects in $Mn_{50}Ni_{32}Sn_7Co_{11}$ alloys. J. Alloys Compd. **832**, 154830 (2020)
40. P. Lázpita, M. Sasmaz, J.M. Barandiarán, V.A. Chernenko, Effect of Fe doping and magnetic field on martensitic transformation of Mn-Ni(Fe)-Sn metamagnetic shape memory alloys. Acta Mater. **155**, 95–103 (2018)

41. L. Zhang, S. Ma, Q. Ge, K. Liu, Q. Jiang, X. Han, S. Yang, K. Yu, Z. Zhong, A systematic study of the antiferromagnetic-ferromagnetic conversion and competition in MnNiGe: Fe ribbon systems. J. Mater. Sci. Technol. **33**, 1362–1370 (2017)
42. H.C. Xuan, Y.Q. Zhang, H. Li, P.D. Han, D.H. Wang, Y.W. Du, The martensitic transformation and magnetic properties in $Ni_{50-x}Fe_xMn_{32}Al_{18}$ ferromagnetic shape memory alloys. Appl. Phys. A **119**, 597–602 (2015)
43. Y. Zhang, L. Zhang, Q. Zheng, X. Zheng, M. Li, J. Du, A. Yan, Enhanced magnetic refrigeration properties in Mn-rich Ni-Mn-Sn ribbons by optimal annealing. Scientific Reports **5**, 11010 (2015)
44. F. Chen, J.L. Sanchez Llamazares, C.F. Sanchez-Valdes, F. Chen, Z. Li, Y.X. Tong, L. Li, Large magnetic entropy change and refrigeration capacity around room temperature in quinary $Ni_{41}Co_{9-x}Fe_xMn_{40}Sn_{10}$ alloys (x= 2.0 and 2.5). J. Alloys Compd. **825**, 154053 (2020)
45. H. Zhang, M. Qian, X. Zhang, L. Wei, F. Cao, D. Xing, X. Cui, J. Sun, L. Geng, Martensite transformation and magnetic properties of Fe-doped Ni-Mn-Sn alloys with dual phases. J. Alloys Compd. **689**, 481–488 (2016)
46. Z.D. Han, D.H. Wang, C.L. Zhang, H.C. Xuan, J.R. Zhang, B.X. Gu, Y.W. Du, Effect of lattice contraction on martensitic transformation and magnetocaloric effect in Ge doped Ni-Mn-Sn alloys. Matter. Sci. Eng. B **157**, 40–43 (2009)
47. N.V. Rama Rao, M.M. Raja, S.E. Muthu, S. Arumugam, S. Pandian, Pressure-magnetic field induced phase transformation in $Ni_{46}Mn_{41}In_{13}$ Heusler alloy. J. Appl. Phys. **116**, 223904 (2014)